# Mutual-Coupling Isolation Using Embedded Metamaterial EM Bandgap Decoupling Slab for Densely Packed Array Antennas

Mohammad Alibakhshikenari[1], *Student Member, IEEE,* Mohsen Khalily[2]*, *Senior Member, IEEE,* Bal S. Virdee[3], *Senior Member, IEEE,* Chan H. See[4,5], *Senior Member, IEEE,* Raed A. Abd-Alhameed[6,7], *Senior Member, IEEE,* and Ernesto Limiti[1], *Senior Member, IEEE*

[1] Electronic Engineering Department, University of Rome "Tor Vergata", Via del Politecnico 1, 00133, Rome, ITALY

[2] Institute for Communication Systems (ICS), Home of the 5G innovation Center (5GIC), University of Surrey, Guildford, GU2 7XH, U.K

[3] London Metropolitan University, Center for Communications Technology & Mathematics, School of Computing & Digital Media, London N7 8DB, UK

[4] School of Engineering and the Built Environment, Edinburgh Napier University, 10 Colinton Road, Edinburgh, EH10 5DT, UK

[5] School of Engineering, University of Bolton, Deane Road, Bolton, BL3 5AB, UK

[6] Faculty of Engineering and Informatics, University of Bradford, Bradford, BD7 1DP, UK

[7] Department of Communication and Informatics Engineering, Basra University, College of Science and Technology, Basra, 61004, Iraq

*Corresponding Author: m.khalily@surrey.ac.uk

***Abstract:*** **This article presents a unique technique to enhance isolation between transmit/receive radiating elements in densely packed array antenna by embedding a metamaterial (MTM) electromagnetic bandgap (EMBG) structure in the space between the radiating elements to suppress surface currents that would otherwise contribute towards mutual coupling between the array elements. The proposed MTM-EMBG structure is a cross-shaped microstrip transmission line on which are imprinted two outward facing E-shaped slits. Unlike other MTM structures there is no short-circuit grounding using via-holes. With this approach, the maximum measured mutual coupling achieved is -60 dB @ 9.18 GHz between the transmit patches (#1 & #2) and receive patches (#3 & #4) in a four-element array antenna. Across the antenna's measured operating frequency range of 9.12 to 9.96 GHz, the minimum measured isolation between each element of the array is 34.2 dB @ 9.48 GHz, and there is no degradation in radiation patterns. The average measured isolation over this frequency range is 47 dB. The results presented confirm the proposed technique is suitable in applications such as synthetic aperture radar (SAR) and multiple-input multiple-output (MIMO) systems.**

***Keyword:*** **Metamaterial, electromagnetic bandgap, array antennas, decoupling slab, mutual coupling, synthetic aperture radar, multiple-input multiple-output.**

## I. INTRODUCTION

In recent years, it has become a necessity to reduce the size of wireless communications systems. However, the size of certain components such as antennas is governed by the wavelength of the signal. Hence, reducing the size of radiating elements in wireless systems has become an area of intense investigation. Antennas are also employed in arrays for applications like multiple-input multiple-output systems where they are prone to detrimental effects of surface waves and near-field, which cause adverse mutual coupling between adjacent *E*-plane coupled microstrip radiating elements. The effect of surface waves becomes especially dominant when the gap between the elements is greater than $0.3\lambda_0$ [1]. Mutual coupling can severely degrade the antenna's radiation characteristics (pattern and efficiency). In addition, mutual coupling can cause correlation between the transmitted and received signals when the antennas are in close-proximity to each other that can result is diminution of system performance [2].

Numerous approaches have been investigated to reduce the mutual coupling between closely located antennas. Examples include using: (i) shorting patches to prevent the excitations of the surface waves [3]; (ii) cavity-backed slots [4]; (iii) partial substrate removal [5]; (iv) planar soft surfaces [6]; (v) parasitic element isolators [7]; (vi) metamaterial insulators for small-size antennas [8, 9]; and (vii) reversal of current through the metamaterial radiators [10].

EM bandgap structures have also been used in planar antennas to improve the antenna's performance [11,12]. EM bandgap structures consist of periodic structures with half-wavelength periodicity separation of dielectric or metal elements that function to prevent propagation of surface waves within its bandgap [13]. The accommodation of half-wavelength periodicity separation in array antennas is physically challenging. Hence, various attempts have been carried out to reduce the size of EM bandgap structures [14–16]. Properties of EM bandgap have been exploited to reduce mutual coupling between antenna elements [17–24].

Wireless transceivers employing full-duplex (i.e. simultaneous transmit/receive) currently employ distinct frequencies for transmit and receive channels. Studies show that by using a single frequency for the full-duplex operation can substantially increase

throughput as well as simplify the front-end architecture of a transceiver [25]. Various other approaches for full-duplex communication have also been investigated previously including optimising the antenna geometry [26–28], using various polarization diversity techniques [29–31], exploiting digital beamforming [32], near-field filtering [33,34], RF-canceller [35], combined mechanical/EBG structures [36] and sharing single antenna [37]. However, there is still a need for small-size antenna configurations with high-isolation between adjacent radiating elements.

In this paper, a technique is described to realise high isolation between antenna elements suitable for array antennas or full-duplex high-speed target radars. The array antenna used to demonstrate this technique consists of four-element patch radiators implemented on the same substrate. The array antenna is designed to operate over 9.12 to 9.96 GHz with bandwidth of 840 MHz, which is extensive band for MIMO and SAR applications. Mutual coupling reduction is achieved by employing a unique metamaterial EM bandgap decoupling slab. Unlike conventional mutual coupling reduction approaches, the proposed technique provides high isolation between radiating elements and the size of the array antenna remains unchanged. The antenna performance and mutual coupling were analysed using standard full-wave EM simulation tools and then were validated by the measurements. In addition, to more validity of the proposed method the results extracted from the full wave EM simulator have compared with the circuit model, which show an excellent agreement with each other proving the precisely of the proposed approach.

## II. Mutual Coupling Reduction Between Array Elements

This section first discusses the basic array antenna used in this study as a reference that is constituted from four square patches with no decoupling slab. Reflection and transmission coefficient response of the array is presented without and with loading of a cross-shaped simple decoupling slab (SDS), which is located between the four radiators, to show the degree of mutual coupling suppression between array's elements. Enhanced suppression is demonstrated in section III by employing MTM electromagnetic bandgap (EMBG) decoupling structure.

### *A. Array Antenna Structure*

The reference array antenna, depicted in Fig. 1, is constructed with four identical square microstrip patches, where each patch is excited individually. Dielectric substrate used is a lossy FR-4 with dielectric constant $\varepsilon_r$= 4.3, thickness $h$ = 1.6 mm and loss-tangent $tan\delta$= 0.025. The configuration of the array antenna is symmetrical.

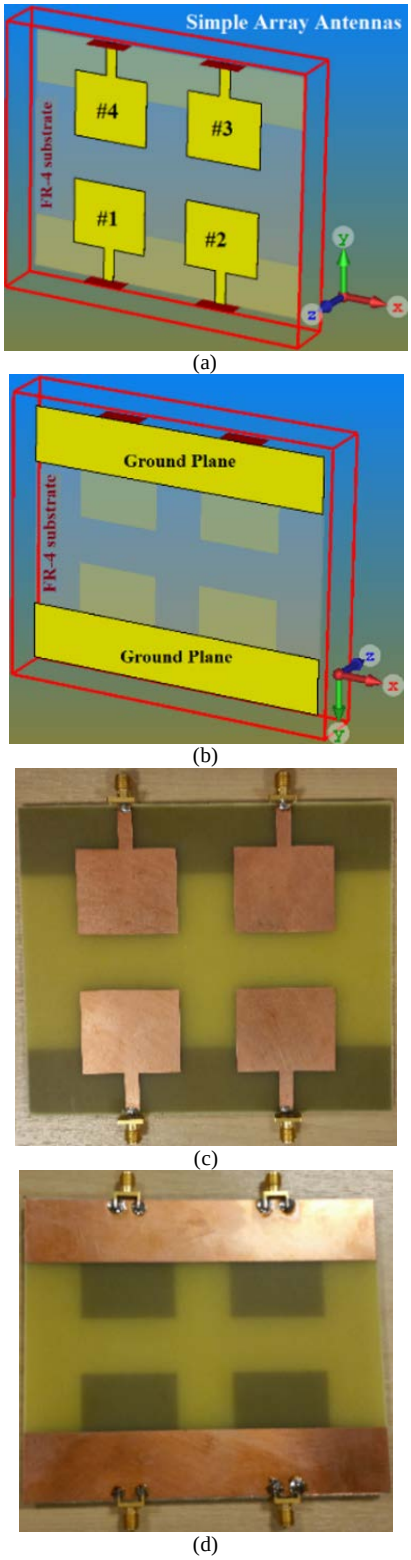


Fig. 1. Reference array antenna configuration using four identical square patches, (a) top view of array antenna comprising four microstrip patches, (b) ground plane of array antenna, (c) fabricated prototype of the antenna, and (d) ground plane view of the fabricated antenna prototype.

Measured S-parameter responses (reflection coefficient ($S_{11}$<-10dB) and transmission coefficients ($S_{12}$, $S_{13}$, & $S_{14}$)) of each radiating element (#1 to #4) of the reference array antenna are shown in Fig. 2. The patch antennas operate from 9.12 GHz to 9.60 GHz with frequency bandwidth, maximum impedance matching

and fractional bandwidth of 480 MHz, -40 dB at 9.36 GHz (resonance frequency), and 5.13%, respectively. The isolation (minimum, average, and maximum) between elements: #1 & #2; #1 & #3; and #1 & #4, are given in Table I. Due to symmetrical configuration of the proposed array antenna, the isolation between other adjacent elements are identical.

### *B. Array Antenna with Simple Decoupling Slab*

The main challenge is to achieve high isolation between the antenna elements while keeping them as close possible to each other to realize a compact array. A simple cross-shaped decoupling slab, shown in Fig. 3, was used to improve the isolation between the radiating elements of the array antenna in Fig. 1. The decoupling slab was inserted between the array's elements, as shown in Fig. 4. In the array antenna, patch #1 & #2 is used for transmission, and #3 & #4 for reception. Ground-plane of the array antenna is truncated as shown in Figs. 4 (b) and 4(d).

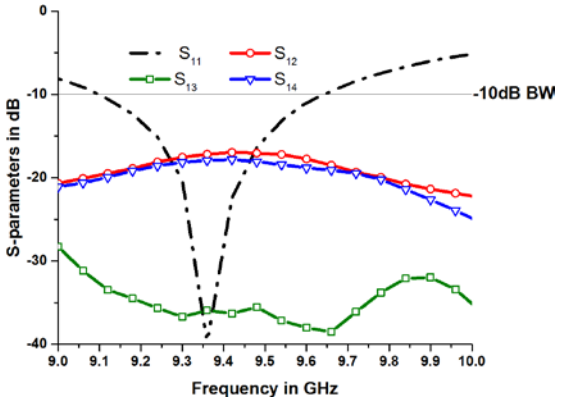


Fig. 2. Measured reflection coefficient ($S_{11}$<-10dB) and transmission coefficients ($S_{12}$, $S_{13}$, & $S_{14}$) of the reference array antenna.

TABLE I: Isolation Between Array Antenna's Elements

| S-parameters | $S_{12}$ | $S_{13}$ | $S_{14}$ |
|---|---|---|---|
| Minimum | 16.95dB @9.42GHz | 34.0dB @9.12GHz | 18.0dB @9.42GHz |
| Average | 19.5 dB | 35.75 dB | 20.0dB |
| Maximum | 21.85dB @9.96GHz | 37.5dB @9.60GHz | 22.0dB @9.96GHz |

The S-parameter performance of the array antenna with the decoupling slab in Fig. 5 shows the array has an impedance bandwidth of 720 MHz from 9.12 to 9.84 GHz, which is corresponds to fractional bandwidth of 7.6%. Comparing Figs. 2 and 5, it is evident by inserting SDS the antenna's bandwidth is extended by 240 MHz. This shows the decoupling slab does not degrade the impedance bandwidth of the array antenna. Optimum impedance match of -25 dB is observed at resonance frequency of 9.37 GHz. By applying the simple decoupling slab, the measured isolation of greater than 10 dB is achieved between the transmit patches (#1 & #2) and receive patches (#3 & #4). The minimum, average, and maximum transition coefficients ($S_{12}$, $S_{13}$, and $S_{14}$) are given in Table II. Due to symmetrical configuration of the proposed array antenna, the isolation between other adjacent elements is identical.

## III. DECOUPLING SLAB WITH EMBEDDED EM BANDGAP

Conventional microstrip antenna are built on dielectric substrates that comprise conductive tracks implemented on the top surface with a conductive ground-plane on the bottom surface of the substrate. It is shown in [38] that only $TM^{odd}$ and $TE^{even}$ modes propagate in a microstrip structure, and the cut-off frequency of $TM^{odd}$ is independent of substrate thickness. It is this mode that propagates through a thin substrate, and along with surface currents contribute towards mutual coupling. The suppression of surface currents between adjacent radiating elements in an array antenna and $TM^{odd}$ mode is therefore necessary to prevent degradation of the radiation pattern in array antennas. EMBG structure shown in Fig. 6 is used here to minimize mutual coupling between neighbouring antennas in the array.

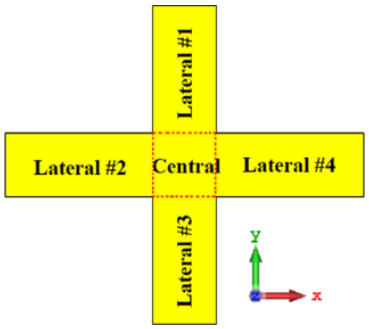


Fig. 3. Simple decoupling slab structure (SDS).

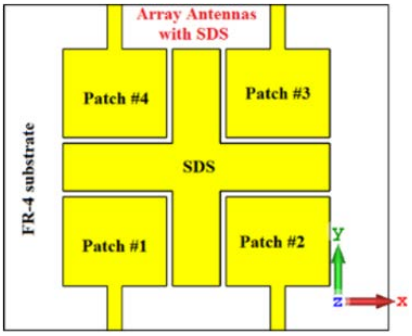


(a)

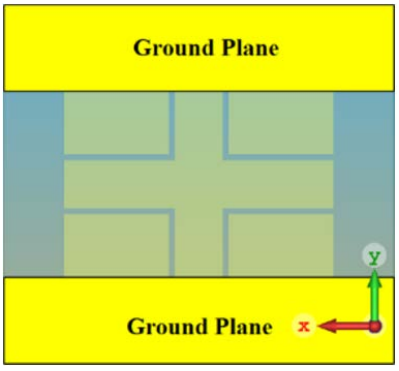


(b)

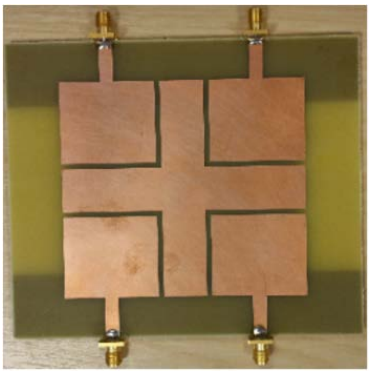

(c)

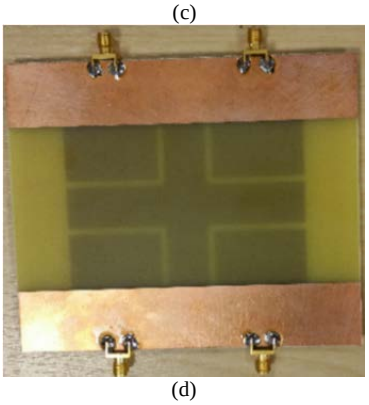

(d)

Fig. 4. Array antenna configuration with embedded SDS, (a) simulated top view, (b) simulated back view of ground-plane, (c) fabricated prototype of the array, and (d) fabricated prototype of the ground plane.

TABLE II: Isolation Between Array Antenna's Elements

| S-parameters | $S_{12}$ | $S_{13}$ | $S_{14}$ |
|---|---|---|---|
| Minimum | 22.0dB @9.84GHz | 30.66dB @9.12GHz | 19.13dB @9.48GHz |
| Average | 27.0dB | 34.52dB | 24.0dB |
| Maximum | 32.0dB @9.12GHz | 38.9dB @9.54GHz | 27.5dB @9.84GHz |

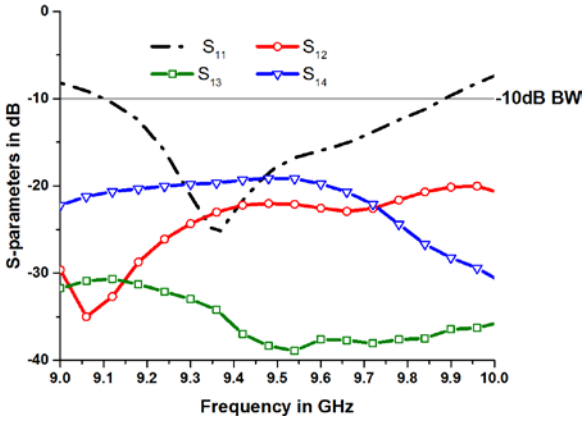


Fig. 5. Measured S-parameters performances of the array antenna with simple decoupling slab.

The proposed MTM-EMBG structure consists of resonant elements that are magnetically coupled to the dominant substrate mode, as shown in Fig. 6. Construction of the EM bandgap isolator involves embedding two identical E-shaped slits in each arm of the conductive decoupling slab of Fig. 3. The slab essentially acts like a shunt inductance, and the two outwards facing E-shaped slits act as a series capacitor. Horizontally polarized magnetic-field coupling the slits induce electric currents on the MTM-EMBG decoupling slab that generate a magnetic-field in the opposite direction. When the E-shaped slits are in close-proximity, the inductance of the slab increases. At resonant frequency, the MTM-EMBG decoupling slab becomes essentially a perfect magnetic conductor that thwarts propagation of the substrate mode. Self-inductance resulting from mutual coupling interaction can be characterised by [39]

$$L_T = \frac{\mu_r \mu_0 A_{strip}}{d} \qquad (1)$$

where $A_{strip}$ is the surface area region bounding the E-shaped slits, and $d$ is the gap between the slits. Horizontal magnetic-fields induce current in the conducting track that generates perpendicular electric-fields at the edges of the slits, and the corresponding capacitance can be calculated using [40]

$$C_T = \varepsilon_r \varepsilon_0 \frac{K(k_T)}{K\left(\sqrt{1-k_T^2}\right)} \qquad (2a)$$

$$k_T = \sin\left(\frac{\pi}{2}\eta\right) + 2\frac{\sqrt{\eta}}{1+\eta} \qquad (2b)$$

Where $\eta$ is the metallization ratio, and $K(k)$ is the complete elliptic integral of first kind defined by [40]

$$\eta = \frac{w_s}{w_s+d} \qquad (2c)$$

$$K(k) = \int_0^{\frac{\pi}{2}} \frac{d\emptyset}{\sqrt{1-k^2 sin^2 \emptyset}} \qquad (2d)$$

Where $w_s$ is width of slits, and $d$ represents gap between them (see Fig. 6). The inductance and capacitance of the EMBG unit-cell at 9.4 GHz is determined to be $L_T = 12.8nH$ and $C_S = 3.5pF$, respectively.

From [39, 40] the transmission-line model for the MTM-EMBG structure is shown in Fig. 7. Inductance of the EM bandgap unit-cell can be represented with an inductive mutual coupling $K_1$. The mutual coupling between two horizontal E-shaped slits is represented by $K_2$. Mutual coupling between the equivalent transmission-line and the E-shaped slits is expressed by capacitive coupling $C_{right}$ and $C_{left}$ corresponding to the right and left slits, respectively. $Q_f$ and $C_p$ represent the quality-factor of the MTM-EMBG structure and the parasitic capacitance between the slab and ground plane, respectively.

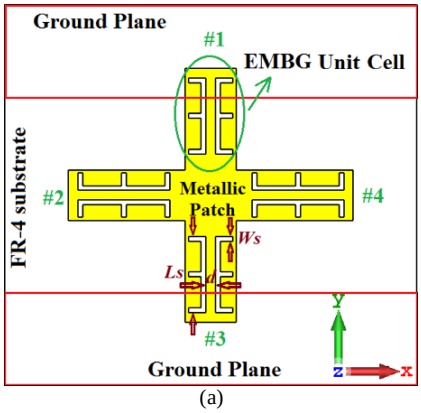


(a)

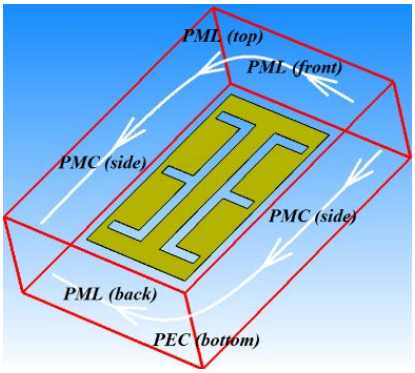


(b)

Fig. 6. (a) Proposed MTM based EMBG decoupling slab embedded with four unit-cells of double E-shaped slits, and (b) EM bandgap unit-cell boundary conditions for full-wave simulation using finite element method solver.

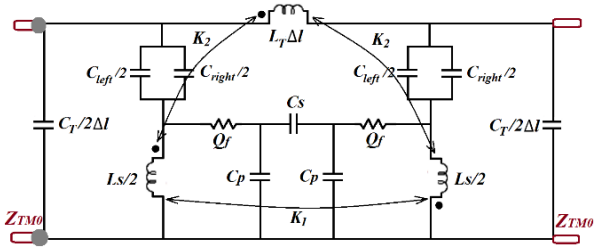


Fig. 7. Transmission-line model of the EM bandgap unit-cell.

To confirm the accuracy of the MTM-EMBG structure model, a 3D EM full-wave solver (CST Microwave Studio ver. 2016) was employed. As shown in Fig. 6(b), the perfect magnetic conductor (PMC) walls impose the boundary conditions around the unit-cells. Perfectly matched layers (PMLs) are assigned to eliminate nonphysical reflections at the boundary of the upper free-space and the front and back sides. Perfect electric conductor (PEC) is assigned at the bottom as ground plane. Equivalent circuit parameters of the MTM-EMBG unit-cell from the 3D EM full-wave solver is given in Table III. This information was then used to determine the equivalent electrical circuit model, shown in Fig. 7, which was verified using Keysight's ADS (RF circuit solver). Fig. 8 shows how the mutual coupling coefficient $K_1$ and $K_2$ are affected with variation in the gap between the E-shaped slits using circuit model and 3D EM full-wave solver. The proposed equivalent circuit model correlates well with the 3D EM full-wave solver results.

TABLE III: Extracted Circuit Elements of the MTM-EMBG Unit-Cell Equivalent Circuit Model

| | |
|---|---|
| $C_S$ | 3.5 $pF$ |
| $L_S$ | 12.8 $nH$ |
| $K_1$ | 0.28 |
| $K_2$ | 0.8 |
| $C_p$ | 4.36 $pF$ |
| $C_{right}$ | 7.95 $pF$ |
| $C_{left}$ | 7.95 $pF$ |
| $Q_f$ | 2.1 Ω |
| $\Delta l$ | 3 mm |
| $Z_{TM0}$ | 50 Ω |

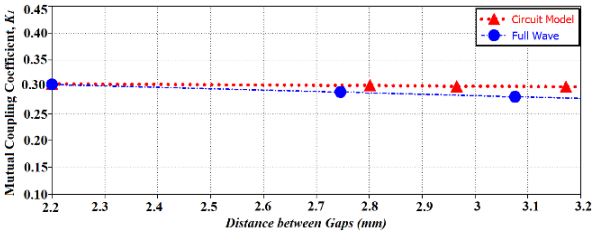


(a)

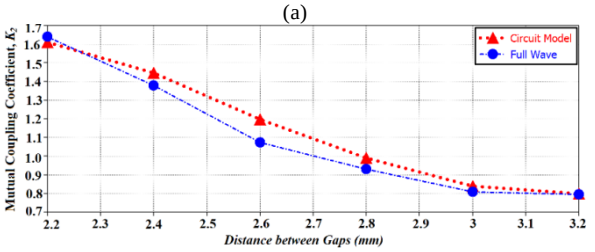


(b)

Fig. 8. Comparison between full-wave and circuit model of coupling coefficients ($K_1$ and $K_2$) as a function of gap between the E-shaped slits, (a) $K_1$, and (b) $K_2$.

Mutual coupling coefficients $K_1$ and $K_2$ describe the magnetic-field linkage between the substrate mode and the EM bandgap isolator, and are dependent on the physical dimensions of the EM bandgap isolator. Fig. 8 shows that as the gap between the unit-cell becomes larger, the mutual coupling between the two E-shaped gaps ($K_2$) becomes weaker; however, the inductive coupling between the substrate mode and the unit-cell ($K_1$) shows little variations to the gap between the slits within the range ($\boldsymbol{\lambda}_g/16 \sim \boldsymbol{\lambda}_g/12$).

Characterisation of the proposed MTM-EMBG decoupling structure can be obtained from simulation of the model in Fig. 9(a). The simulated surface impedance is shown in Fig. 9(b). It can be observed the MTM-EMBG decoupling structure exhibits acceptable impedance over its operational frequency range from 8.8 to 10.5 GHz. The reflection coefficients are shown in Fig. 9(c). The results show the decoupling structure design is optimum at ~9.85 GHz.

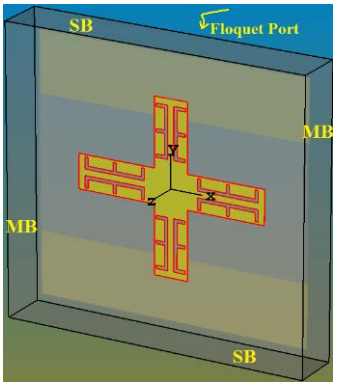


(a)

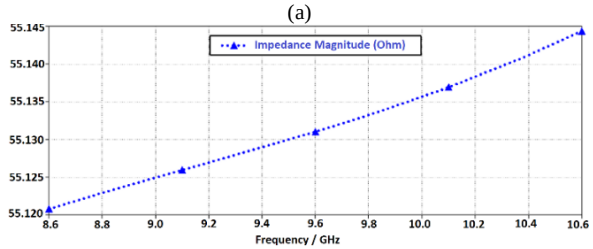


(b)

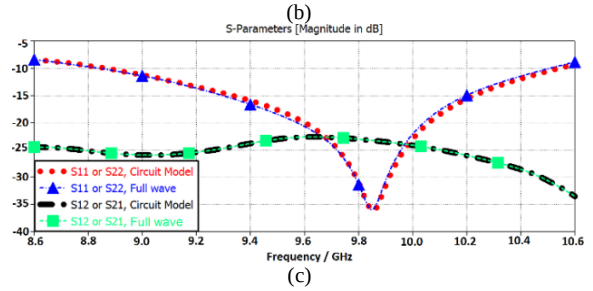


(c)

Fig. 9. The proposed MTM EM bandgap decoupling structure etched on the top side of the substrate and excited by 50Ω microstrip transmission line on the bottom of the substrate: (a) Simulation model for determining the characteristics of the MTM-EMBG decoupling structure with slot width and length of $W_s$=1.5mm and $L_s$=24mm, respectively. Note, MB and SB represent the master and slave boundaries, respectively; (b) Simulated surface impedance of the MTM-EMBG decoupling structure; and (c) Simulated and circuit model reflection and transmission coefficients of the MTM-EMBG decoupling structure.

## IV. Array Antenna With MTM-EM Bandgap Isolator

Functionality of the proposed MTM-EMBG decoupling slab is demonstrated with a four-element antenna array, where the cross shaped decoupling slab is inserted between the patch antenna arrangement, as shown in Fig. 10(a), where Antennas #1 & #2 are used for transmission (TX), and Antennas #3 & #4 are used for reception (RX) in a RF transceiver. The ground-plane on the back side of the substrate is truncated, as shown in Fig. 10(b). The distance between the adjacent radiating elements ($d_1$) and gap between the elements and the decoupling slab ($d_2$) are 20 mm ($0.6\lambda_0$) and 2 mm ($0.06\lambda_0$), respectively, where $\lambda_0$ is the free space wavelength at 9.12 GHz.

The MTM-EMBG decoupling slab was designed for optimum performance at 9.6 GHz. The equivalent circuit model of the vertical unit-cell coupled to patch#1 & #2 is shown in Fig. 10(e). The equivalent circuit of other unit-cells coupled with adjacent patch antennas is similar. Value for *RLC* parameters are: 5.2 Ω, 11.5 nH, and 7.8 pF, respectively. The decoupling slab has a slot width of $W_s$ = 1.5 mm and slot length of $L_s$= 24 mm. Dimensions of the array antenna are given in Fig. 11.

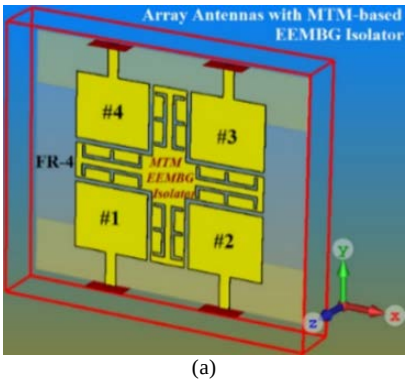


(a)

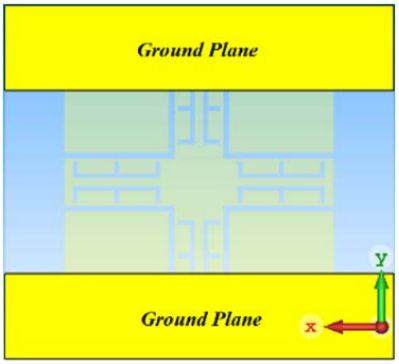


(b)

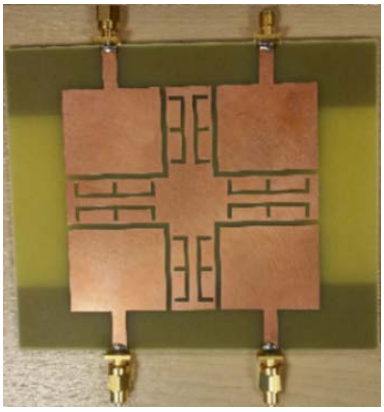

(c)

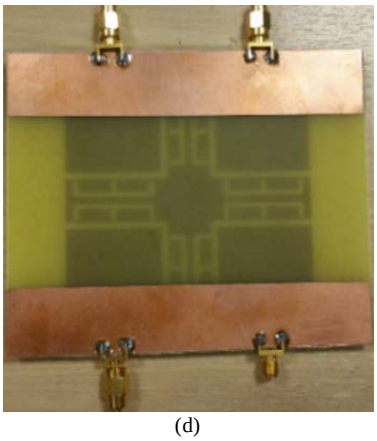

(d)

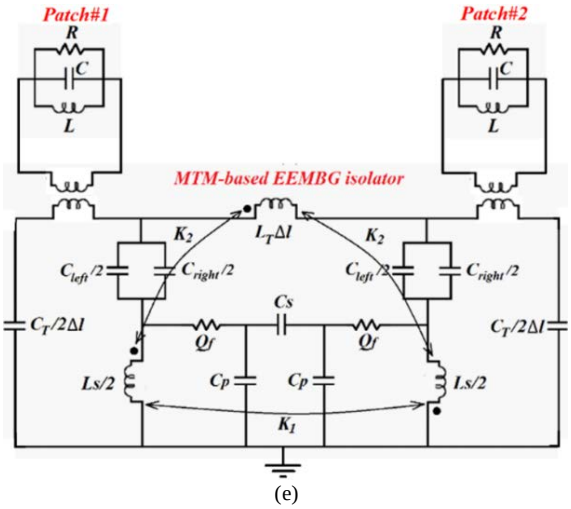


(e)

Fig. 10. Geometry of the array antenna with MTM-EM bandgap decoupling slab, (a) simulated top view, (b) simulated bottom view of ground-plane, (c) fabricated prototype of the array, (d) fabricated prototype of the ground plane, and (e) the equivalent circuit model of the vertical unit-cell interfaced with patch antennas #1 and #2.

The antenna's S-parameter responses are depicted in Fig. 12. The bandwidth of the array antenna is 840 MHz (9.12 GHz to 9.96 GHz), with a fractional bandwidth of 8.8%. The bandwidth has extended by 360 MHz. Besides the reflection coefficients, the magnitude of the transition coefficients ($S_{12}$, $S_{13}$, and $S_{14}$) have substantially dropped. The minimum, average, and maximum magnitudes for $S_{12}$ are: -34.2 dB, -47 dB, and -60 dB; for $S_{13}$ they are -28.33 dB, -36.12 dB, and -44.3 dB; and for $S_{14}$ they are -27 dB, -30 dB, and -33 dB. For clarity these results are given in Table IV. The proposed structure's optimum performance is at 9.6 GHz with impedance matching of -15.0 dB. At this frequency the antenna's isolation between elements #1 & #2, #1 & #3, and #1 & #4 are 38.2 dB, 38.2 dB, and 30.15 dB, respectively. This reveals greater than 10 dB improvement in isolation compared with the reference antenna at 9.6 GHz between the transmit patches (#1 & #2) and receive patches (#3 & #4). Due to symmetrical configuration of the proposed array antenna, the isolation between other adjacent elements is identical.

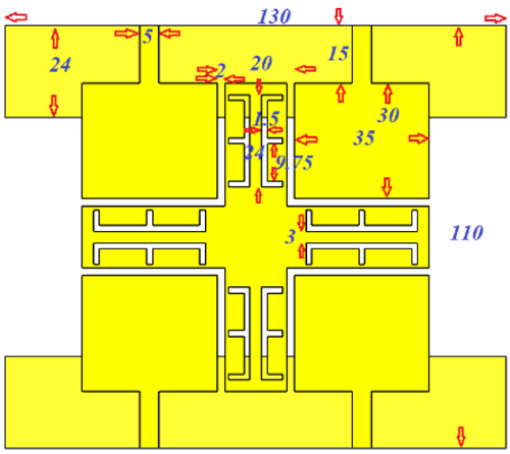


Fig. 11. Dimensions (in millimetre) of the proposed antenna array with MTM EM bandgap isolator.

TABLE IV: Isolation Between Array Antenna's Elements

| S-parameters | $S_{12}$ | $S_{13}$ | $S_{14}$ |
|---|---|---|---|
| Minimum | 34.2dB @9.48GHz | 28.33dB @9.12GHz | 27.0dB @9.42GHz |
| Average | 47.0dB | 36.12dB | 30.0dB |
| Maximum | 60.0dB @9.18GHz | 44.3dB @9.72GHz | 33dB @9.12GHz |

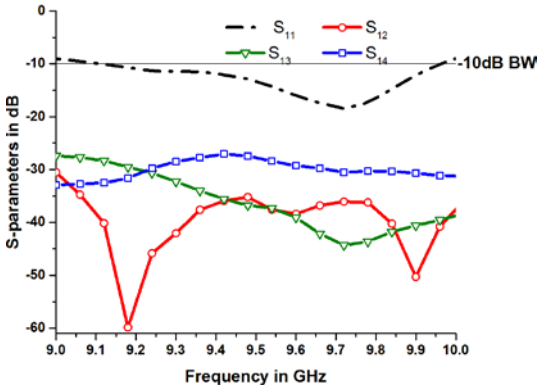


Fig. 12. Measured S-parameters of the array antenna with MTM EM bandgap decoupling slab.

The measured S-parameter responses without decoupling slab (reference case), with SDS, and with MTM-EMBG decoupling slab are shown in Fig.13. It is evident that with MTM-EMBG, (i) the reflection coefficient is better than −15 dB at around 9.6 GHz; and (ii) improvement in the impedance bandwidth is greater than 350 MHz. It's worth to mention that, the resonance frequencies for the reference antenna without decoupling slab and the antenna with simple decoupling slab are same. However, it has shifted to the high frequency after applying the metamaterial decoupling slab. The reason is that, when we have realized the metamaterial properties by etching the E-shaped slots on the decoupling slab the series left-handed capacitances have generated that enhance the capacitive property of the entire structure, which is caused to shift the resonance frequency to higher frequency.

Surface wave suppression functionality of the MTM-EMBG decoupling slab is evident in the experimental transmission coefficient ($S_{12}$) response between antenna elements #1 & #2, shown in Fig. 13(a). MTM-EMBG decoupling slab has a significant effect on whole of the frequency bandwidth from 9.12 – 9.96 GHz. At 9.18 GHz, the difference in isolation is more than 40 dB and at 9.6 GHz the isolation deteriorates to more than 20 dB. This is because the MTM-EMBG unit-cell has a finite operational bandwidth. Due to symmetrical configuration of the array antenna the transmission coefficient between elements #3 & #4 is identical to between elements #1 & #2 (i.e. $S_{34} = S_{12}$). The measured transmission coefficient response between elements #1 & #3, and elements #1 & #4 with and without MTM-EMBG are shown in Figs. 13(b) and 13(c), respectively. It is clear from Fig. 13(b) that, the MTM-EMBG decoupling slab has moderate effect at higher frequencies and the isolation tends to converge between

9.4 and 9.6 GHz. The measured transmission coefficient between elements #1 & #4 are shown in Fig. 13(c), which is identical to between elements #2 & #3 ($S_{23} = S_{14}$). At 9.18 GHz, the difference in isolation is 15 dB, and at 9.6 GHz the isolation is 12 dB. These results clearly show the effectiveness of the MTM-EMBG decoupling structure in reducing the mutual coupling between adjacent antennas encountered in array antennas. The results are summarized in the Table V. It should be noted in the proposed technique no short-circuit grounding using via-holes has been used. Due to the symmetrical configuration of the proposed array antenna, the magnitude of $S_{11}$ is identical to $S_{22}$, $S_{33}$, and $S_{44}$. Also, $S_{12}=S_{34}$, $S_{13}=S_{24}$, and $S_{14}=S_{23}$.

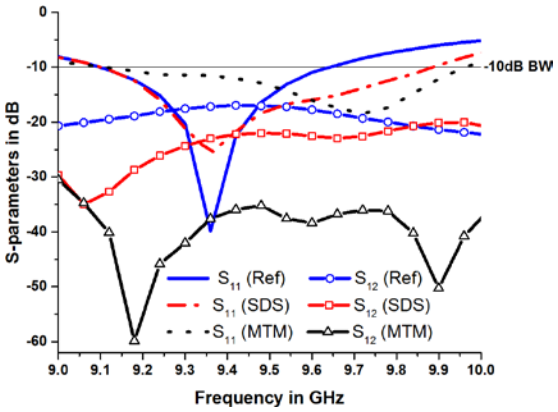


(a) Due to the symmetrical configuration of the proposed array antenna the results are same for elements #1 and #2.

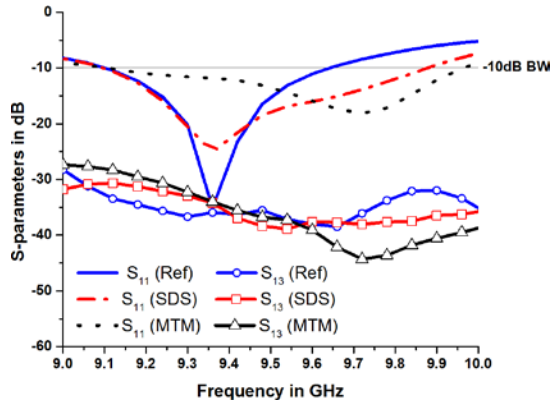


(b) Due to the symmetrical configuration of the proposed array antennas the results are same for elements #1 and #3.

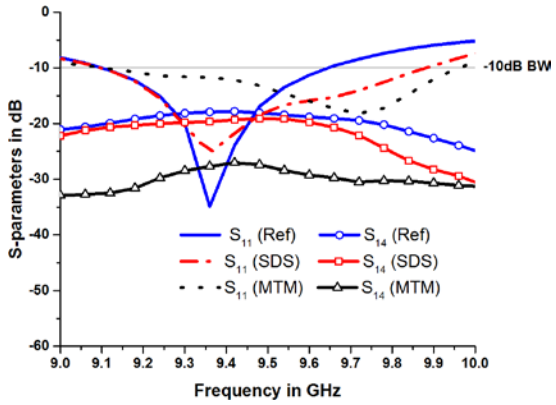


(c) Due to the symmetrical configuration of the proposed array antenna the results are same for elements #1 and #4

Fig. 13. Measured S-parameter responses of the proposed array antennas before and after applying MTM-EMBG isolator, (a) between elements #1 & #2, (b) between elements #1 & #3, and (c) between elements #1 & #4.

Current density distribution over the array antenna with and without MTM-EMBG decoupling slab is shown in Fig.14. It is evident from these plots the MTM-EMBG decoupling slab soaks up the fringing fields that would otherwise couple with the adjacent radiating elements.

The measured radiation patterns of four-element array antennas under the all three conditions (reference antenna with no loading, SDS and MTM-EMBG loadings) at 9.18 GHz, 9.4 GHz and 9.6 GHz are shown in Fig. 15. It is observed the radiation patterns with MTM-EMBG decoupling slab approximates the original reference antenna, and over certain angular directions can exhibit better gain performance. The maximum gain of the array antenna with the decoupling slab increased from 3.3 dBi to 5.4 dBi corresponding to 63% improvement.

TABLE V. S-Parameter Characteristics of the Proposed Array Antenna

| **$S_{11}$, $S_{22}$, $S_{33}$, $S_{44}$ <-10 dB** | Average matching | Max. matching | Bandwidth | Fractional BW |
|---|---|---|---|---|
| Reference Array | -25dB | -40dB @ 9.36GHz | 9.12 – 9.6 GHz | 5.13% |
| With SDS | -17.5dB | -25.76dB @ 9.36GHz | 9.12 – 9.84 GHz | 7.6% |
| With MTM-EMBG | -14.5dB | -18.45dB @ 9.72GHz | 9.12 – 9.96 GHz | 8.80% |

| **$S_{12}$ & $S_{34}$** | Min. isolation | Average isolation | Max. isolation |
|---|---|---|---|
| Reference Array | 16.95dB @ 9.42GHz | 19.5dB | 21.85dB @ 9.96GHz |
| With SDS | 22dB @ 9.84 GHz | 27dB | 32dB @ 9.12GHz |
| With MTM-EMBG | 34.2dB @ 9.48GHz | 47dB | 60dB @ 9.18GHz |

| **$S_{13}$ & $S_{24}$** | Min. isolation | Average isolation | Max. isolation |
|---|---|---|---|
| Reference Array | 34dB @ 9.12GHz | 35.75dB | 37.5dB @ 9.60GHz |
| With SDS | 30.66dB @ 9.12GHz | 34.52dB | 38.9dB @ 9.54GHz |
| With MTM-EMBG | 28.33dB @ 9.12GHz | 36.12dB | 44.3dB @ 9.72GHz |

| **$S_{14}$ & $S_{23}$** | Min. isolation | Average isolation | Max. isolation |
|---|---|---|---|

| | | | |
|---|---|---|---|
| Reference Array | 18.0dB @ 9.42GHz | 20.0dB | 22.0dB @ 9.96GHz |
| With SDS | 19.13dB @ 9.48GHz | 24.0dB | 27.5 @ 9.84GHz |
| With MTM-EMBG | 27.0dB @ 9.42GHz | 30dB | 33dB @ 9.12GHz |

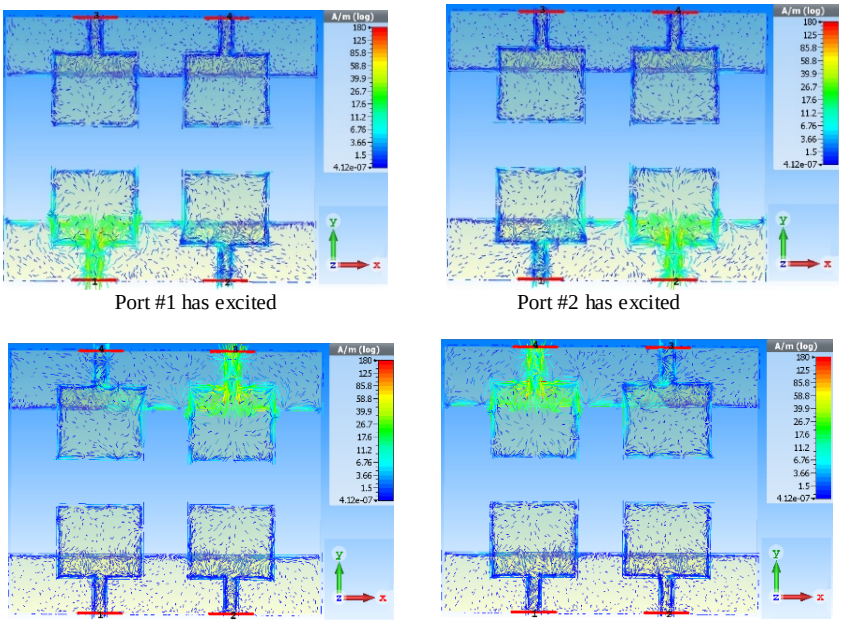

Port #1 has excited Port #2 has excited

Port #3 has excited Port #4 has excited

(a) Current density over the array antenna without decoupling slab

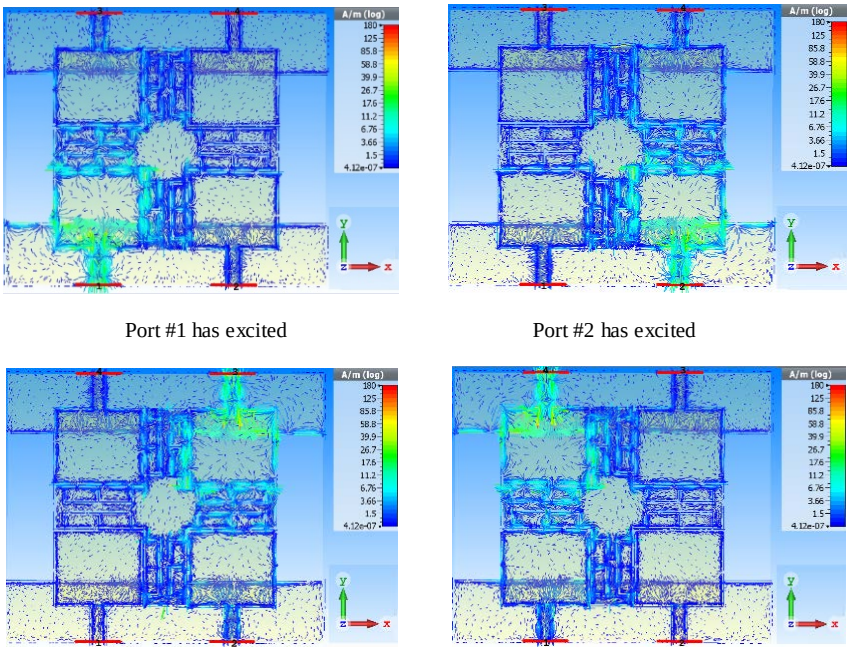

Port #1 has excited Port #2 has excited

Port #3 has excited Port #4 has excited

(b) Current density over the array antenna with MTM-EMBG decoupling slab

Fig.14. Current density over the array antenna at 9.6 GHz, (a) with no MTM-EMBG decoupling slab, and (b) with MTM-EMBG decoupling slab.

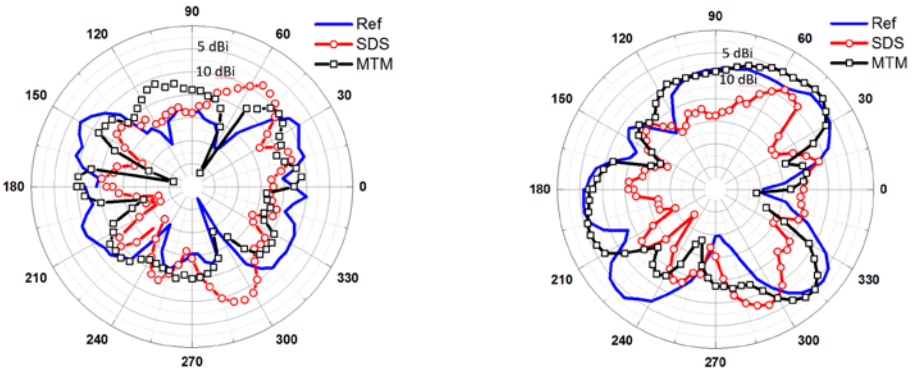


@ 9.18 GHz

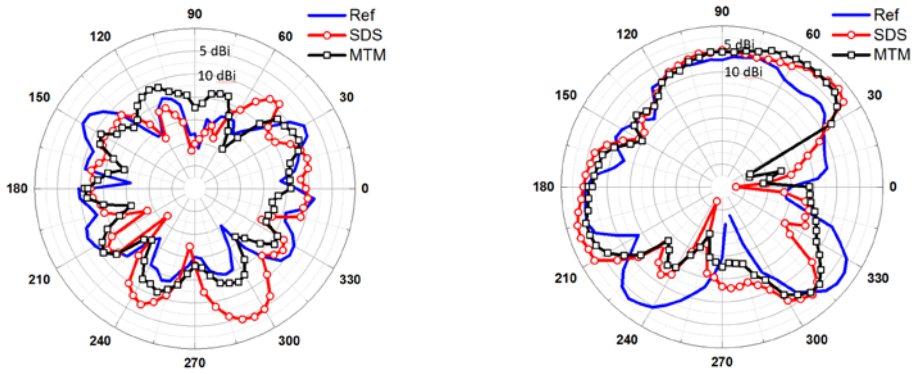


@ 9.4 GHz

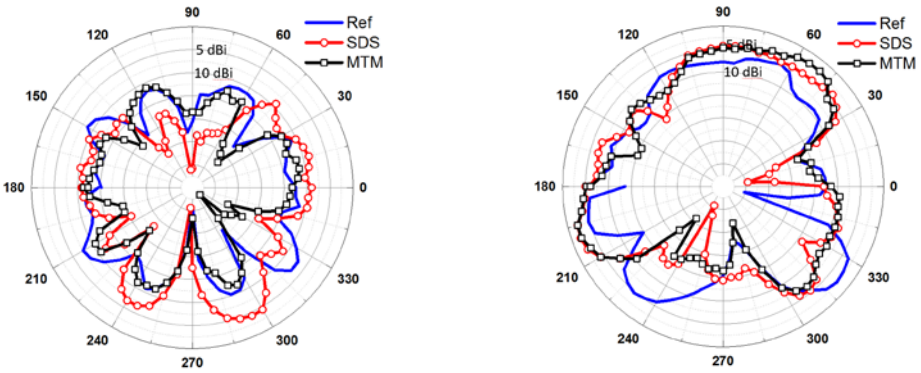


@ 9.6 GHz

Fig.15. Measured radiation patterns of the array antennas, i.e. reference, with SDS, and with MTM-EMBG, at the operational frequencies of 9.18, 9.4, and 9.6 GHz. Please note with reference to Fig. 1(a) the left-hand plots are in the x-y plane and the right-hand plots are in the y-z plane.

## V. COMPARISONS WITH OTHER ANTENNAS

The proposed array antenna is compared with the several recent works in Table VI. In the literature, all the proposed designs are constructed with only two radiation elements, since they have not symmetrical configuration that impossible them to realize the arrays with more than two elements. However, in our case due to the symmetrical configuration of the structure we have increased the array elements to four. All papers referenced in Table VI have defected ground plane to enhance isolation between the two radiating elements, which caused to enhance complexity of the structure and therefore the cost for manufacture procedures has increased. With the proposed technique the size of the array antenna remains unchanged. The maximum isolation improvement between adjacent antennas with the proposed method is 40 dB, which is comparable to [41], however unlike [41] in the proposed technique there is no need to temper with the ground plane, and the MTM-EMBG decoupling structure didn't require short-circuit vias. This resulted in a simple technique which can be retrofitted to existing antenna arrays quickly and at low cost for MIMO systems and SAR applications.

TABLE VI. Proposed Antenna Characteristics Compared with Recent Works

| Refs. | Technique | Max. Isolation Improvement | Number of Elements | Symmetricity | Impact on the Size after apply MTM | Changing and Developing (defected ground plane) | Complexity |
|---|---|---|---|---|---|---|---|
| [17] | UC-EBG | 10 dB | 2 (1×2) | NO | Yes | Yes | Yes |
| [41] | Slot in Ground plane | 40 dB | 2 (1×2) | NO | Yes | Yes | Yes |
| [42] | EBG | 4 dB | 2 (1×2) | NO | Yes | Yes | Yes |
| [43] | Compact EBG | 17 dB | 2 (1×2) | NO | Yes | Yes | Yes |
| [44] | DGS | 17.43 dB | 2 (1×2) | NO | Yes | Yes | Yes |
| [45] | U-shaped resonator | 10 dB | 2 (1×2) | NO | Yes | Yes | Yes |
| [46] | Slotted Meander Line Resonator | 16 dB | 2 (1×2) | NO | Yes | Yes | Yes |
| [47] | I-shaped resonator | 30 dB | 2 (1×2) | NO | Yes | Yes | Yes |
| [48] | SCSRR | 10 dB | 2 (1×2) | NO | Yes | Yes | Yes |
| [49] | SCSSRR | 14.6 dB | 2 (1×2) | NO | Yes | Yes | Yes |
| [50] | Waveguide MTM | 20 dB | 2 (1×2) | NO | Yes | Yes | Yes |
| [51] | Waveguide MTM | 18 dB | 2 (1×2) | NO | Yes | Yes | Yes |
| [52] | Meander line resonator | 10 dB | 2 (1×2) | NO | Yes | Yes | Yes |
| [53] | Fractal load with DGS | 16 dB | 2 (1×2) | NO | Yes | Yes | Yes |
| [54] | Antenna Interference Cancellation Chip (AICC) | 15 dB | 2 (1×2) | Yes | No | No | Yes |
| [55] | 3-D Metamaterial Structure (3DMMS) | 18 dB | 2 (1×2) | Yes | Yes | No | No |
| **This work** | **Metamaterial** | **40 dB for $S_{12}$ ~7 dB for $S_{13}$ 11 dB for $S_{14}$** | **4 (2×2)** | **Yes** | **NO** | **NO** | **NO** |

## VI. CONCLUSIONS

A novel technique is demonstrated to suppress mutual coupling between adjacent radiating elements in array antennas. This involves inserting a metamaterial electromagnetic bandgap decoupling structure between the radiating elements. The proposed MTM-EMBG structure, which does not require any via-holes and defected ground plane structures, can be directly implemented on the surface of the planar array antenna. In addition, the MTM-EMBG structure can also be retrofitted with ease. Experimental results show excellent isolation is achieved with the decoupling slab across 9.12 to 9.96 GHz. The results confirm the proposed technique is suitable in applications such as synthetic aperture radar (SAR) and multiple-input multiple-output (MIMO) systems.

## ACKNOWLEDGEMENTS

This work is partially supported by innovation programme under grant agreement H2020-MSCA-ITN-2016 SECRET-722424 and the financial support from the UK Engineering and Physical Sciences Research Council (EPSRC) under grant EP/E022936/1.

## REFERENCES

[1] Jedlicka, R.P., Poe, M.T., Carver, K.R.: 'Measured mutual coupling between microstrip antennas', *IEEE Trans. Antennas Propag.*, Vol.29, pp. 147–149, 1981.

[2] Pozar, D.M., Schaubert, D.H.: 'Analysis of an infinite array of rectangular microstrip patches with idealized probes feeds', *IEEE Trans. Antennas Propag.*, Vol. 32, No.10, pp. 1101–1107, 1984.

[3] Amendola, G., Boccia, L., Massa, G.: 'Shorted elliptical patch antennas with reduced surface waves on two frequency bands', *IEEE Trans. Antennas Propag.*, Vol. 53, No.6, pp. 1946–1956, 2005.

[4] Hikage, T., Omiya, M., Itoh, K.: 'Performance evaluation of cavity-backed slot antennas using the FDTD technique', *Proc. of IEEE Antennas and Propag. Society Int. Symp.*, Vol. 3, pp. 1484–1487, 2000.

[5] Yeap, S.B., Chen, Z.N.: 'Microstrip patch antennas with enhanced gain by partial substrate removal', *IEEE Trans. Antennas Propag.*, Vol. 58, No.9, pp. 2811–2816, 2010.

[6] Iglesias, E.R., Quevedo-Teruel, O., Inclán-Sánchez, L.: 'Planar soft surfaces and their application to mutual coupling reduction', *IEEE Trans. Antennas Propag.*, Vol.57, No.12, pp. 3852–3859, 2009.

[7] Zhang, S., Khan, S., He, S.: 'Reducing mutual coupling for an extremely closely-packed tunable dual-element PIFA array through a resonant slot antenna formed in-between', *IEEE Trans. Antennas Propag.*, Vol.58, No.8, pp. 2771–2776, 2010.

[8] Buell, K., Mosallaei, H., Sarabandi, K.: 'Metamaterial insulator enabled superdirective array', *IEEE Trans. Antennas Propag.*, Vol.55, No.4, pp. 1074–1085, 2007.

[9] Trindade, D.V.B.M., Muller, C., De Castro, M.C.F., et al.: 'Metamaterials applied to ESPAR antenna for mutual coupling reduction', *IEEE Ant. Wirel. Propag. Lett.*, Vol.14, pp. 1622–1625, 2014.

[10] Abdalla, M., Ibrahim, A.: 'Design of close, compact, and high isolation metamaterial MIMO antennas'. *2013 IEEE AP-S Int. Antenna and Propagation Symp. Dige*st, Orlando, USA, pp. 186–187, July 2013.

[11] C. Chang, Y. Qian, and T. Itoh, 'Analysis and applications of uniplanar compact photonic bandgap structures', *Progress in Electromagnetic Research, PIER*, Vol. 41, pp. 211–235, 2003.

[12] H. J., Xu, Y. H. Zhang, and Y. Fan, 'Analysis of the connection between K connector and microstrip with electromagnetic bandgap (EBC) structures', *Progress in Electromag. Res., PIER*, 2007, 73, pp. 239–247.

[13] Rahmat-Samii, Y., Mosallaei, H.: 'Electromagnetic band-gap structures: classification, characterization, and applications'. *Proc. of Inst. of Electrical Engineering – ICAP Symp.*, pp. 560–564, April 2001.

[14] Zhang, S., Lau, B.K., Tan, Y., et al.: 'Mutual coupling reduction of two PIFAs with a T-shape slot impedance

transformer for MIMO mobile terminals', *IEEE Trans. Ant. Propag.*, Vol. 60, No.3, pp. 1521–1531, 2012.
[15] Abdelreheem, A.M., Abdalla, M.A.: 'A novel bilateral UC-EBG structure', *IEEE Ant. and Propag. Society Int. Symp.*, pp. 1780–1781, 2014.
[16] Zheng, Q.R., Fu, Y.Q., Yuan, N.C.: 'A novel compact electromagnetic bandgap (EBG) structure', *IEEE Trans. Antennas Propag.*, Vol.56, No.6, pp. 1656–1660, 2008.
[17] Farahani, H.S., Veysi, M., Kamyab, M., et al.: 'Mutual coupling reduction in patch antenna arrays using a UC-EBG superstrate', *IEEE Antennas Wirel. Propag. Lett.*, Vol. 9, pp. 57–59, 2010.
[18] Exposito-Dominguez, G., Fernandez-Gonzalez, J.-M., Padilla, P., et al.: 'Mutual coupling reduction using EBG in steering antennas', *IEEE Antennas Wirel. Propag. Lett.*, Vol. 11, pp. 1265–1268, 2012.
[19] Rajo-Iglesias, E., Quevedo-Teruel, Ó., Inclan-Sanchez, L.: 'Mutual coupling reduction in patch antenna arrays by using a planar EBG structure and a multilayer dielectric substrate', *IEEE Trans. Antennas Propag.*, Vol. 56, No.6, pp. 1648–1655, 2008.
[20] Payandehjoo, K., Abhari, R.: 'Employing EBG structures in multiantenna systems for improving isolation and diversity gain', *IEEE Antennas Wirel. Propag. Lett.*, Vol. 8, pp. 1162–1165, 2009.
[21] Iluz, Z., Shavit, R., Bauer, R.: 'Microstrip antenna phased array with electromagnetic bandgap substrate', *IEEE Trans. Antennas Propag.*, Vol.52, No.6, pp. 1446–1453, 2004.
[22] Assimonis, S.D., Yioultsis, T.V., Antonopoulos, C.S.: 'Computational investigation and design of planar EBG structures for coupling reduction in antenna applications', *IEEE Trans. Magn.*, Vol. 48, No.2, pp. 771–774, 2012.
[23] Lombart, N., Neto, A., Gerini, G., et al.: '1-D scanning arrays on dense dielectrics using PCS-EBG technology', *IEEE Trans. Antennas Propag.*, Vol.55, No.1, pp. 26–35, 2017.
[24] Mohamed, I.S., Abdalla, M.A.: 'Reduced size mushroom like EBG for antennas mutual coupling reduction'. *32th National Radio Science Conf. (NRSC 2015)*, Egypt, pp. 57–62, 2015.
[25] S. Goyal, P. Liu, S. Hua. S. Panwar, 'Analyzing a full-duplex cellular system,' *47th Annual Conference on Information Sciences and Systems (CISS)*, pp. 1-6, 2013.
[26] Etellisi, E.A., Elmansouri, M.A., Filipovic, D.S., 'Wideband monostatic simultaneous transmit and receive (STAR) antenna', *IEEE Trans. Antennas Propag.*, Vol.64, No.1, pp. 6–15, 2016.
[27] Tianang, E.G., Filipovic, D.S.: 'A dipole antenna system for simultaneous transmit and receive,' *2015 IEEE Int. Symp. on Antennas and Propagation*, pp. 428–429, July 2015.
[28] Etellisi, E.A., Elmansouri, M.A., Filipovic, D.S.: 'Wideband simultaneous transmit and receive (STAR) bi-layer circular array', *2015 IEEE Int. Symp. on Antennas and Propag.*, pp. 2227–2228, 2015.
[29] Dinc, T., Chakrabarti, A., Krishnaswamy, H.: 'A 60 GHz CMOS full-duplex transceiver and link with polarization-based antenna and RF cancellation', *IEEE J. Solid-State Cir.*, Vol.51, No.5, pp. 1125–1140, 2016.
[30] Dinc, T., Krishnaswamy, H.: 'A T/R antenna pair with polarization-based wideband reconfigurable self-interference cancellation for simultaneous transmit and receive', *Proc. of IEEE IMS'15*, pp. 1–4, 2015.
[31] Yetisir, E., Chen, C.-C., Volakis, J.: 'Low-profile UWB 2-port antenna with high isolation', *IEEE Antennas Wirel. Propag. Lett.*, Vol.13, pp. 55–58, 2014.
[32] Snow, T., Fulton, C., Chappell, W.J.: 'Transmit–receive duplexing using digital beamforming system to cancel selfinterference', *IEEE Trans. Microw. Theory Tech.*, Vol. 59, No.12, pp. 3494–3503, 2011.
[33] Wegener, A.: 'Broadband near-field filters for simultaneous transmit and receive in a small two-dimensional array', *IEEE Proc. of Int. Microwave Symp.*, pp. 1–3, June 2014.
[34] Wegener, A., Chappell, W.: 'High isolation in antenna arrays for simultaneous transmit and receive', *IEEE Int. Symp. on Phased Array Systems Technology*, pp. 593–597, Oct. 2013.
[35] Kolodziej, K.E., McMichael, J.G., Perry, B.T.: 'Multitap RF canceller for inband full-duplex wireless communications', *IEEE Trans. Wirel. Commun.*, vol 15, No.6, pp. 4321–4334, 2015.
[36] Niroo-Jazi, M., Denidni, T.A., Chaharmir, M.R., et al.: 'A hybrid isolator to reduce electromagnetic interactions between Tx/Rx antennas', *IEEE Antennas Wirel. Propag. Lett.*, Vol.13, pp. 75–78, 2014.
[37] Reiskarimian, N., Krishnaswamy, H.: 'Magnetic-free non-reciprocity based on staggered commutation', *Nat. Commun.*, pp. 1–10, 2016.
[38] Y. J. Song and K. Sarabandi: 'Equivalent circuit model for metamaterial-based electromagnetic band-gap isolator', IEEE *Antennas and Wireless Propag. Letters*, Vol. 11, pp. 1366-1369, 2012.
[39] H. Mosallaei and K. Sarabandi: 'Design and modeling of patch antenna printed on magneto-dielectric embedded-circuit metasubstrate', *IEEE Trans. Antennas Propag.*, Vol. 55, No.1, pp. 45–52, 2007.
[40] R. Igreja and C. J. Dias, 'Analytical evaluation of the interdigital electrodes capacitance for a multi-layered structure', *Sensors Actuat. A, Phys.*, Vol. 112, pp. 291–301, 2004.
[41] OuYang, J., F. Yang, and Z. M. Wang: 'Reduction of mutual coupling of closely spaced microstrip MIMO antennas for WLAN application,' *IEEE Ant. & Wirel. Propag. Lett.*, Vol. 10, pp.310-312, 2011.
[42] Yu, A. and X. Zhang: 'A novel method to improve the performance of microstrip antenna arrays using a dumbbell EBG structure,' *IEEE Antennas Wireless Propagation Letters*, Vol. 2, No. 1, pp.170-172, 2003.
[43] Islam, M. T. and M. S. Alam: 'Compact EBG structure for alleviating mutual coupling between patch antenna array elements,' *Progress In Electromagnetics Research*, Vol. 137, pp.425-438, 2013.
[44] Zhu, F. G., J. D. Xu, and Q. Xu: 'Reduction of mutual coupling between closely packed antenna elements using defected ground structure,' *Electronics Letters*, Vol. 45, No. 12, pp.601-602, 2012.
[45] Farsi, S., D. Schreurs, and B. Nauwelaers: 'Mutual coupling reduction of planar antenna by using a simple microstrip u-section,' *IEEE Ant. and Wirel. Propag. Lett.*, Vol. 11, pp.1501-1503, 2012.
[46] Alsath, M. G., M. Kanagasabai, and B. Balasubramanian: 'Implementation of slotted meander line resonators for isolation enhancement in microstrip patch antenna arrays,' *IEEE Antennas and Wireless Propagation Letters*, Vol. 12, pp.15-18, 2013.
[47] Ghosh. C. K. and S. K. Parui: 'Reduction of mutual coupling between E-shaped microstrip antennas by using a simple microstrip I-section,' *Microwave & Optical Tech. Letters*, Vol. 55, No. 11, pp.2544-2549, 2013.
[48] Suwailam, M. M. B., O. F. Siddiqui, and O. M. Ramahi: 'Mutual coupling reduction between microstrip patch antennas using slotted-complementary split-ring resonators,' *IEEE Antennas Wireless Propagation Letters*, Vol. 9, pp.876-878, 2010.
[49] Shafique, M. F., Z. Qamar, L. Riaz, R. Saleem, and S. A. Khan: 'Coupling suppression in densely packed microstrip arrays using metamaterial structure,' *Microwave and Optical Technology Letters*, Vol. 57, No. 3, pp.759-763, 2015.
[50] Yang, X. M., X. G. Liu, X. Y. Zhu, T. J. Cui: 'Reduction of mutual coupling between closely packed patch antenna using waveguide metamaterials,' *IEEE Ant. & Wirel. Prop. Lett.*, Vol.11, pp.389-391, 2012.
[51] Qamar, Z. and H. C. Park: 'Compact waveguided metamaterials for suppression of mutual coupling in microstrip array,' *Progress in Electromagnetic Research*, Vol. 149, pp.183-192, 2014.

[52] Jeet Ghosh, Sandip Ghosal, Debasis Mitra, and Sekhar Ranjan Bhadra Chaudhuri, 'Mutual coupling reduction between closely placed microstrip patch antenna using meander line resonator", *Progress in Electromag. Research Lett*.,Vol. 59, pp.115-122, 2016.
[53] Xu Yang, Ying Liu, Yun-Xue Xu, and Shu-xi Gong: 'Isolation enhancement in patch antenna array with fractal UC-EBG structure and cross slot,' *IEEE Antennas Wireless Propagation Letters*, Vol. 16, pp. 2175-2178, 2017.
[54] Luyu Zhao, Feng Liu, Xiumei Shen, Guodong Jing, Yuan-Ming Cai, and Yingsong Li ,"A high-pass antenna interference cancellation chip for mutual coupling reduction of antennas in contiguous frequency bands", *IEEE Access*, vol.6, pp. 38097-38105, 2018.
[55] Kai Yu, Yingsong Li, and Xiaoguang Liu, "Mutual coupling reduction of a MIMO antenna array using 3-D novel meta-material structures", *Applied Computational Electromagnetics Society Journal*, vol.33, no.7, pp.758-763, 2018.